CHAPTER X

OTHER COARSENING SYSTEMS

In this chapter we briefly consider two two dimensional systems that coarsen in a manner that appears qualitatively similar to coarsening in the soap froth and in metals: bubble patterns in the liquid-gas phase transition in lipid monolayers and in the magnetic domains of doped iron garnets. Both are distinguished by the presence of long range interactions which lead to a greater variety of phenomena than observable in normal coarsening. Both are also only beginning to be studied experimentally, with few hard theoretical results. Indeed, in the case of the magnetic bubbles it is still not clear what sort of theory is appropriate.

X.a Lipid Monolayers

If we distribute a small quantity of a lipid surfactant on a water surface, the polar lipid molecules align with their heads at the surface of the fluid and their long polymer tails in the air. Depending on the areal density of the lipid and the temperature, "solid", liquid or gaseous two-dimensional phases may form. We can visualize the phase transition if we add a small amount of a second lipid with a tail marked by a fluorescent dye, the fluorescent group being active only in the liquid phase regions. Illuminating the liquid surface with light of the dye excitation frequency then makes it straightforward (with correct filtering) to observe the patterns of the different phase domains, a technique pioneered by Lösche and Möhwald, and McConnell, Tamm and

gas condenses and the interface grows. If we assume that the total surface energy is small compared to bulk energy, then the temperature and pressure of the lipid remain essentially constant (provided the water temperature is carefully controlled). Since we remain at the same point in the coëxistence curve, the total area of liquid and gas remains constant. Since the thermal diffusion time is long compared to the molecular diffusion time, the patterns are well equilibrated, with minimal surface (circular) shapes. Thus the basic mechanisms driving the pattern evolution are similar to those in coarsening.

A fundamental difference from the soap froth is that , since pressure is carried by the connected matrix phase as well as by the fragmented bubble phase, interactions between bubbles can be long range. When the separation between bubbles is small compared to their size we would expect this effect to be small. When the bubbles are well separated it should dominate, and the behavior should be closer to that of Ostwald ripening.

Depending on the point in the coëxistence region chosen, we can obtain either bubbles of gas in a liquid matrix, bubbles of liquid in a gas matrix, or mixtures of both (e.g. patterns with regions of both types, or hierarchical patterns with gas bubbles inside liquid bubbles, inside gas bubbles, etc.). This range of initial patterns is a fascinating topic in its own right which we will not discuss here. Moore *et al.* studied stearic acid monolayers, looking at gas bubbles in a liquid matrix.[169] They were particularly interested in the possible analogy with the two dimensional soap froth. Qualitatively the phenomena they observed seemed very much like those seen in a soap

froth. The pattern itself looked similar to soap bubbles, with small bubbles shrinking and large bubbles growing. They observed both $T1$ (side swapping) and $T2$ processes (bubble disappearance). The overall length scale of the pattern increased monotonically in time. An obvious difference from the soap froth was the variable width of the walls. At short times bubbles were more round than polygonal, becoming progressively more polygonal with time (a behavior more typical of nucleation than coarsening). Quantitatively, they measured the side distribution for their patterns and the mean bubble area versus time. They obtained a growth exponent of $\alpha = 1.1 \pm 0.1$ (See Table 4), in agreement with the expected value for ideal grain growth. Their measured distribution function is rather tail heavy including a thirteen-sided bubble (See Tables 7 and 8), and depends on measurements of only about forty bubbles. They note that the second moment of the distribution was still increasing at the end of their run, a sure indication that they had not yet reached a scaling state. A problem with lipid monolayer patterns is that, because they form by a nucleation process, they tend to start with many very small bubbles and very broad area distributions and therefore take a long time (and a large relative increase in length scale) to equilibrate. The experiment is much faster than in the soap froth since the typical timescales are a few hours and the absolute length scales typically 10 μm to 100 μm. Even so, maintaining temperature and concentration stability over that time is difficult.

Berge *et al.* have recently extended Moore *et al.*'s work, studying gas

bubbles in a liquid matrix using pentadecanoic acid, with a hexadecylamine label.[29] Unfortunately experimental difficulties with image stability and analysis have so far prevented them from making quantitative measurements, but they did observe coarsening with well defined $T1$ and $T2$ processes for a wide range of ratios of matrix area to bubble area. For patterns dominated by bubbles, the evolution looked very similar to that of the soap froth, with walls of uniform width and polygonal bubbles (See Fig. 52). For patterns with more matrix the bubbles were rounder (See Fig. 53) and some ambiguity crept in in determining the number of sides (See Fig. 54), though it is always possible to formally determine nearest neighbors using the Voronoi construction. In the former case the rates of growth appeared to be close to von Neumann's law, in the latter, the rate of shrinkage of small bubbles appeared to depend on the bubbles' size as well as their number of sides. In patterns with extremely narrow walls, wall breakage and grain coalescence occured, but were rare otherwise. Glazier has measured side distributions from ordered ($N = 221$) and disordered ($N = 103$) patterns supplied by Berge (See Tables 7 and 8 and Fig. 55).[92] The "disordered" pattern probably still contained some residual order but its side distribution lay within the experimental range for the scaling state soap froth. On the basis of these observations we may tentatively conclude that the narrow matrix lipid monolayer behaves like an ideal two dimensional coarsening system. The crucial piece of missing information is the dynamics, a measurement of the dependence of the growth rate for bubbles on their number of sides and size.

Fig. 52 Lipid Monolayer Bubbles. Pattern of lipid monolayer bubbles showing well separated round bubbles (Figure supplied by B. Berge 1989).

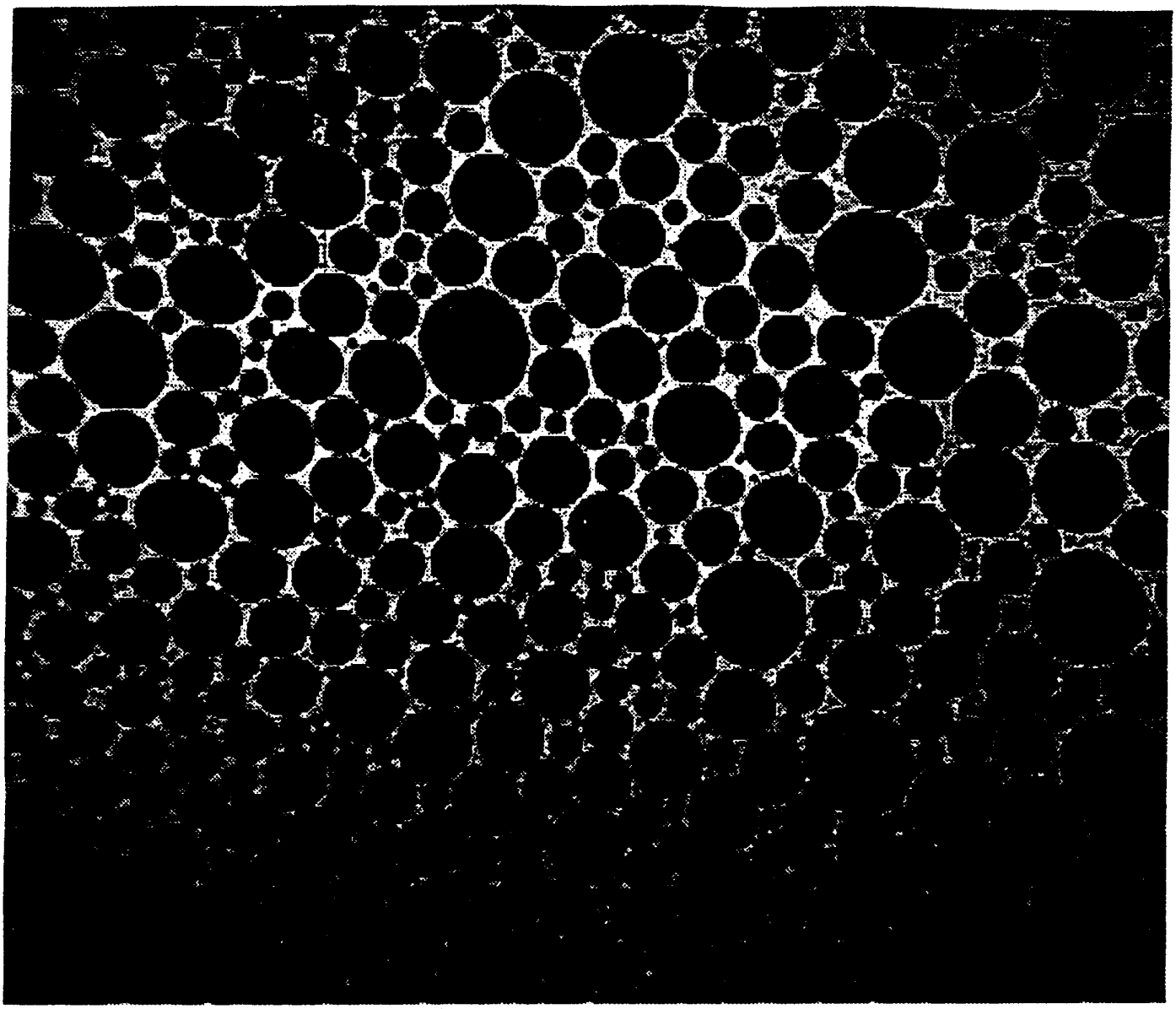

Fig. 53 Lipid Monolayer Bubbles. Pattern of lipid monolayer bubbles showing close packed polygonal bubbles (Figure supplied by B. Berge 1989).

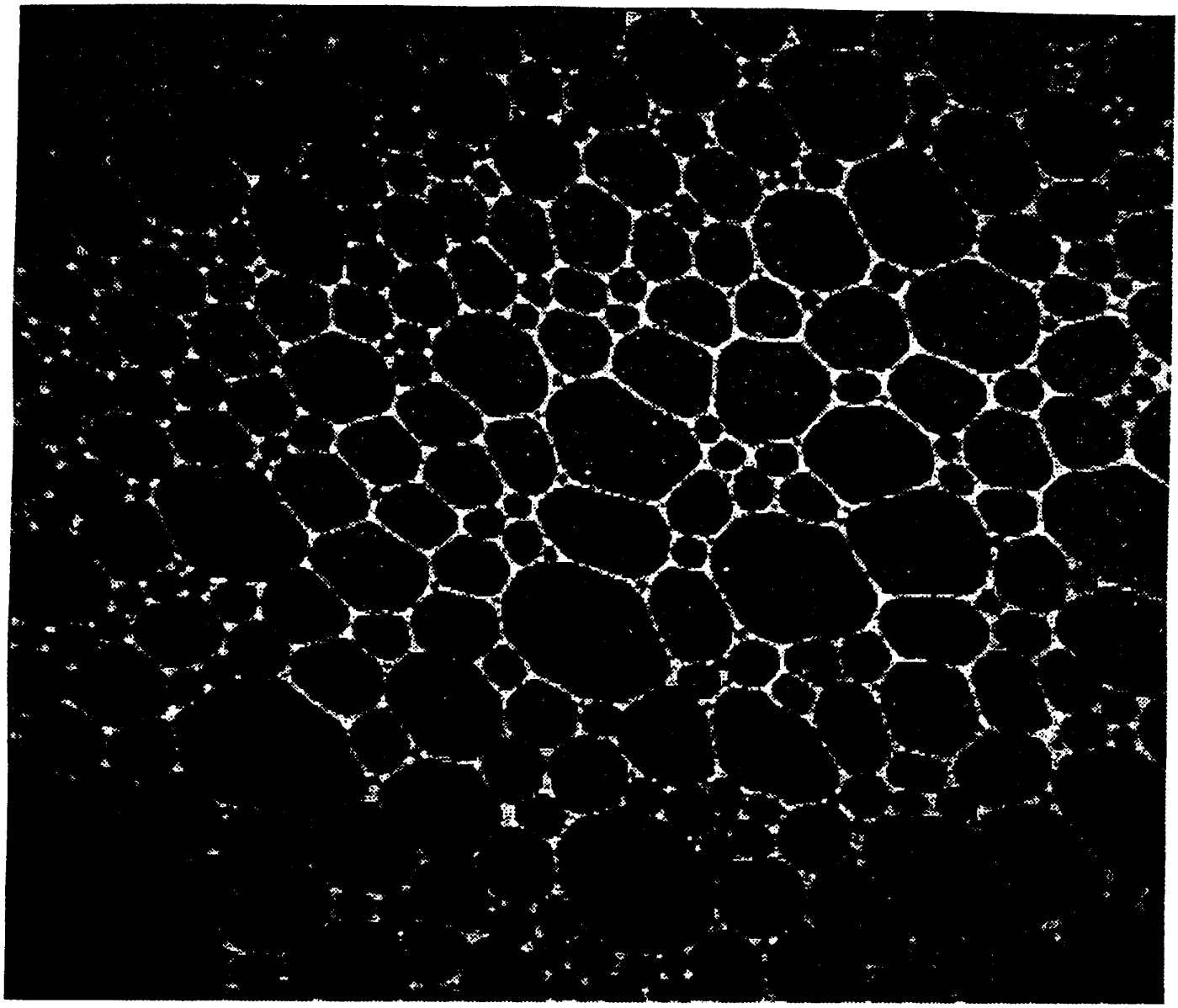

Fig. 54 Ambiguity in Separated Bubbles. (a) A four-sided bubble. (b) A three-sided bubble. In some situations only the Voronoi construction can to distinguish the two cases.

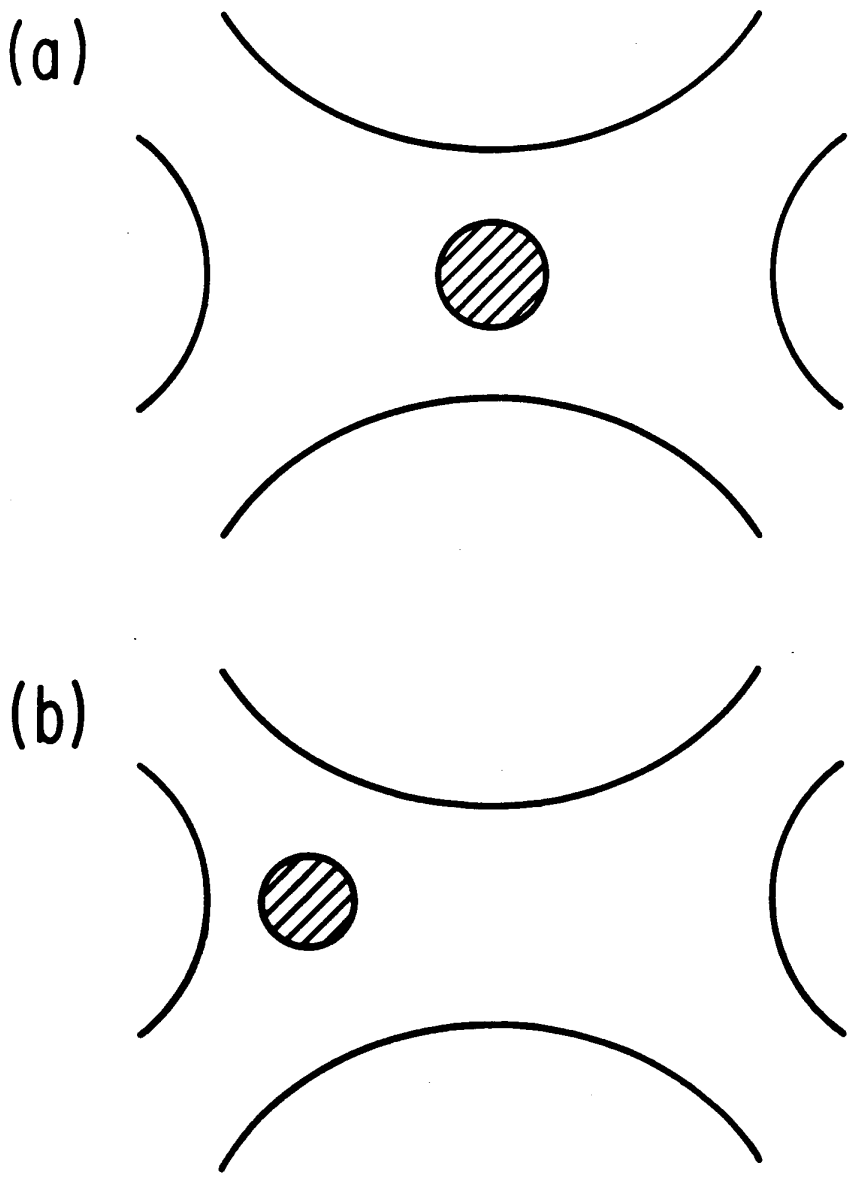
(a)
(b)

Fig. 55 Side Distribution. Side distribution for an ordered and a disordered lipid monolayer pattern. A typical soap froth distribution is given as a comparison.

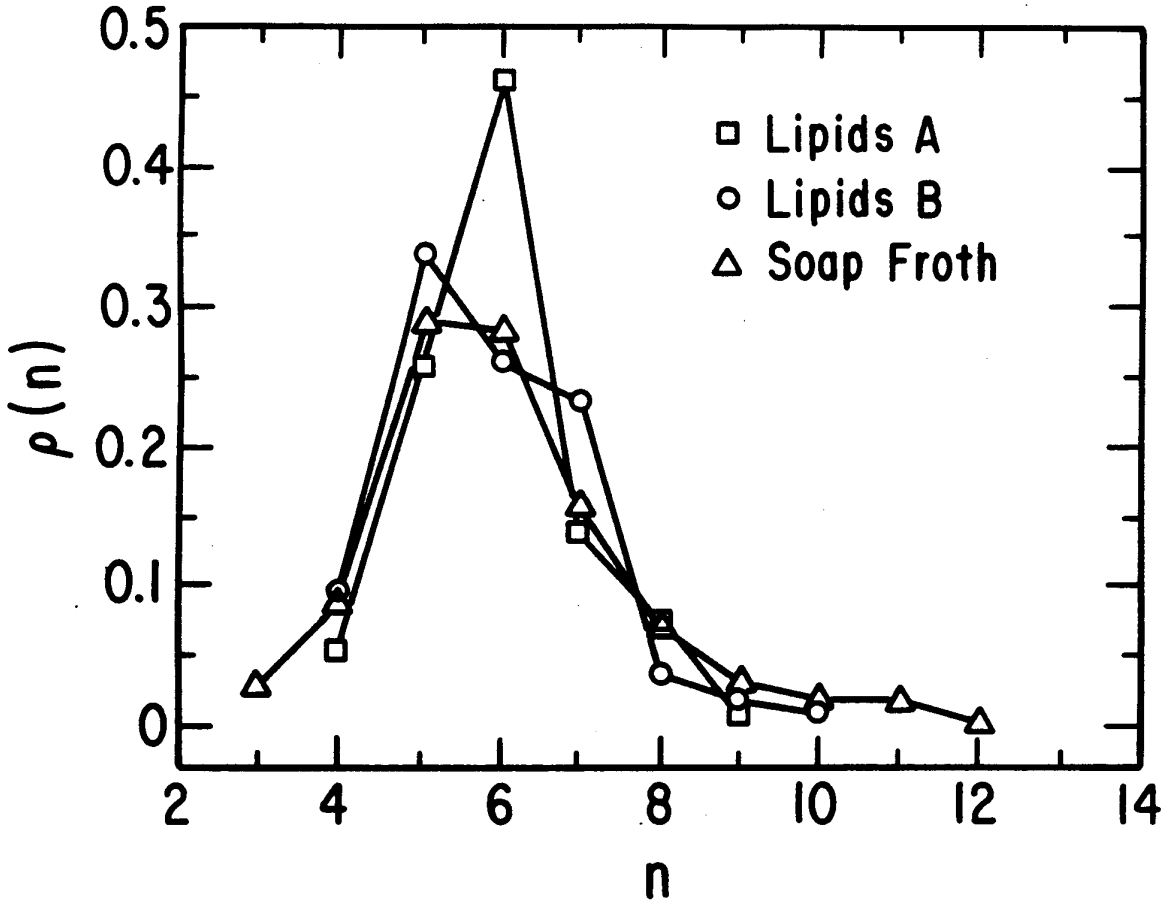
0.5
0.4
0.3
0.2
0.1
0
ρ(n)
2
4
6
8
10
12
14
n
Lipids A
Lipids B
Soap Froth

Based on our concept of the lipid monolayer as intermediate between the soap froth and Ostwald ripening, we suggest that a reasonable form for the growth rate should be:

$$\frac{dA(n,r)}{dt} = (1-\epsilon)\kappa(n-6) + \epsilon\frac{\kappa}{2\pi}(1 - \frac{r}{< r >}), \qquad \text{(X.1)}$$

where ϵ is a fitting parameter that describes the degree of polygonality of the bubbles, being zero for purely polygonal bubbles, and one for infinitely separated bubbles. The form of the second term comes from the requirement that area be conserved. We can easily rewrite any of our mean field and network models using this sort of a fundamental dynamics. We could also write a next order theory to include the dependence of a bubble on the properties of its neighbors, in which we explicitly consider area exchange between all pairs of bubbles:

$$\frac{dA_i}{dt} = (1-\epsilon)\kappa(n_i-6) + \epsilon\frac{\kappa}{2\pi}\sum_j f(|\vec{x}_i - \vec{x}_j|)(\frac{1}{r_j} - \frac{1}{r_i}), \qquad \text{(X.2)}$$

where i indexes the bubbles, $\vec{x}_i$ is the position of the center of the ith bubble and f describes the drop off with distance of the interaction between bubbles. We might also wish to make ϵ a local function of bubble size and separation. Without further experimental data we cannot begin to discuss correlations in side redistribution, local fluctuations, or other second order effects.

X.b Magnetic Bubbles

Throughout our previous discussion we have examined coarsening in time, the basic mechanism in all cases being diffusion driven by energy gra-

dients. Magnetic bubble patterns, in contrast, are usually time independent, with the control parameter being the strength of an applied magnetic field. Generally when the applied magnetic field changes, the pattern evolves rapidly and then reaches a time independent state (sometimes with a few noise driven adjustments at later times). This difference of control parameter allows a variety of experiments impossible in normal coarsening, since it allows us to move "backwards in time" towards smaller length scales. Further complications come in two types. The long range interactions in magnetic systems are longer range and less intrinsically self averaging and support larger gradients than in lipid monolayers. They are also fundamentally nonlinear, which makes them harder to model.

The magnetic bubble patterns that we will discuss are regions of particular spin orientation in thin samples of doped ferri-magnetic iron garnets. The anisotropy of the material is such that the spins tend to align either up or down perpendicular to the material. When viewed in a microscope under crossed polarizers, the Faraday effect makes one spin orientation look light and the other dark. Since the basic exchange interaction is ferromagnetic, like spins clump into macroscopically large patches of a given orientation, and the patterns are easy to visualize.

Because they were once thought to have industrial applications, iron garnet magnetic bubble materials have been studied extensively by engineers and applied physicists.[31,45,63,186,224] There have been analytic calculations of the behavior of isolated bubbles and regular bubble lattices as well as

pattern instabilities.[156,187,212,225,226,235,253] There are a number of interesting questions concerning residual twists in domain walls (Bloch lines), and various kinds of anisotropy which need not concern us directly here.

While a full Hamiltonian for a magnetic bubble pattern would be difficult to write down (and even a moderately complete one is complicated) we need concern ourselves with only a few terms.[63] An applied magnetic field will tend to align spins with it. The domain walls between regions of reversed spin have an energy associated both with the mismatch between neighboring spins and with the local spin misalignment relative to the crystal as the spins rotate (spatially) from one orientation to the other. Finally, regions of uniform spin orientation have a dipole energy created by the self-interaction with the total generated field. In schematic form we may express this as an Hamiltonian:[63]

$$\mathcal{H} = \sum_i \left(-\vec{\sigma}_i \cdot \vec{\mathrm{H}} - \sum_{neighbors\ i} 2J\vec{\sigma}_i \cdot \vec{\sigma}_j \right) + J' \int_{Area} \sin^2(\psi(\vec{x}))d\vec{x} + 2\pi \int_{Area} \mathrm{M}^2(\vec{x})d\vec{x}, \tag{X.3}$$

where i indexes the spins, $\vec{\sigma}_i$ is a spin, J is a positive exchange strength, J' an anisotropy strength, ψ the angular mismatch between local spin orientation and the preferred crystalline orientation, $\vec{\mathrm{H}}$ the applied magnetic field, and M the local magnetization per unit area. The four terms correspond respectively to the external field energy, the exchange energy, the anisotropy energy, and the dipole energy.

The basic mechanism controlling the formation of magnetic bubble patterns is the competition between the wall energy which favors the creation

of large domains, and the dipole energy which favors the creation of small domains. Thus the basic dynamics differ from the soap froth in the presence of long range forces. Also if the size of the domains is very small, the wall energy per unit area is very large. If the domains are very large, the dipole energy per unit area is very large. Thus for any given value of the external magnetic field (and control parameters like temperature) the pattern has a preferred wavelength which minimizes the sum of the wall and dipole energies. The wall energy has the additional function of a surface tension, tending to straighten (or reduce to smooth arcs) the domain walls. Because of the presence of long range forces we cannot expect rigorous minimal surfaces however. Recurved walls reminiscent of metal grains are also common. The applied magnetic field controls the balance between the two spin orientations and also increases the preferred wavelength.

If the sample is raised above the temperature at which it undergoes its ferrimagnetic phase transition (the Néel temperature, T_N, is approximately 130° C in Molho *et al.*'s samples) and is then cooled, it forms at zero field (depending on the individual sample and the applied field when the Néel temperature is crossed on cooling) one of two basic types of pattern, a more or less regular array of bubbles (See Fig. 57 (A)), or a continuous folded labyrinth (See Fig. 56 (a)).

If we apply a magnetic field to the labyrinth favoring one spin orientation (by convention we will assume that we favor the white spins in our pictures), the black regions first narrow and then begin to unwind, keeping close to

Fig. 56 Coarsening of a Labyrinth. Stages in the coarsening of a magnetic bubble labyrinth subject to an external magnetic field. (a) H= 0 Oe. (b) H= 1470 Oe. (c) H= 2250 Oe. (d) H= 2700 Oe. (e) H= 3080 Oe. (f) H= 3300 Oe (From Kooy and Enz 1960).[124]

(a)

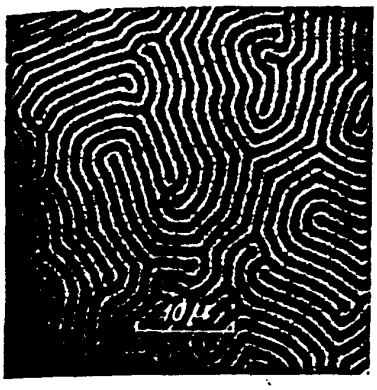

(b)

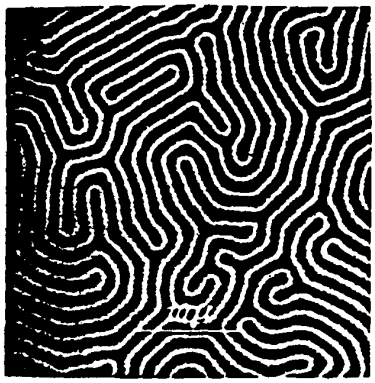

(c)

(d)

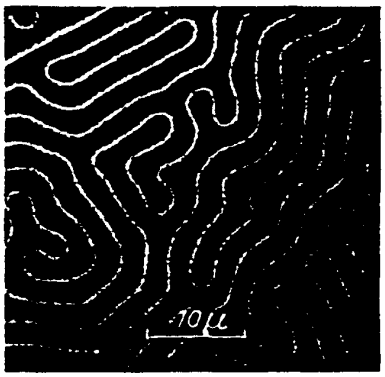

(e)

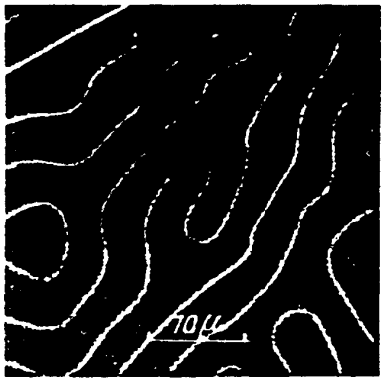

(f)

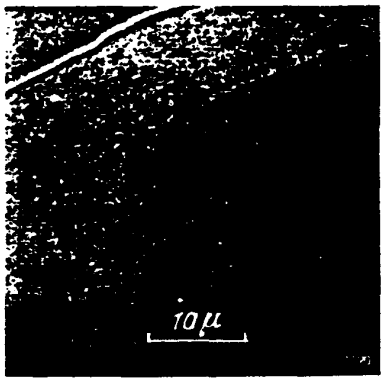

Fig. 57 Coarsening of Magnetic Bubbles. Normal coarsening at $T = 20°$ C of a magnetic bubble pattern with applied magnetic field. (A) H= 0 Oe. (B) H= 54.1 Oe. (C) H= 73.8 Oe. (D) H= 85.2 Oe (Figure supplied by P. Molho 1989).

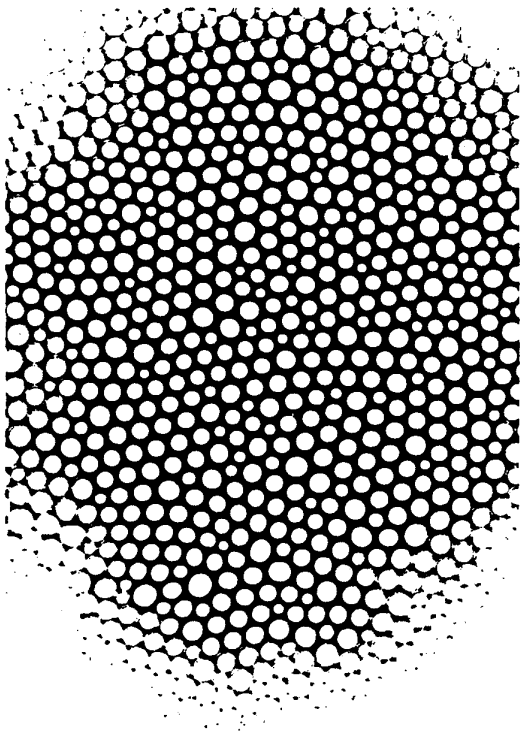

(A)

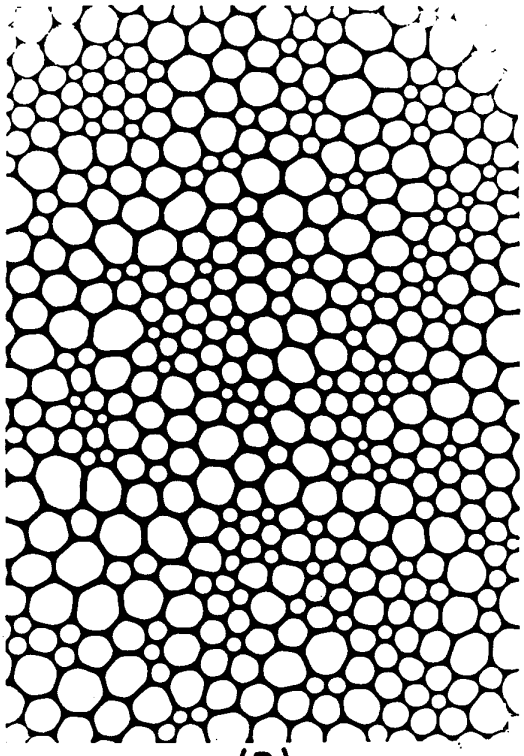

(B)

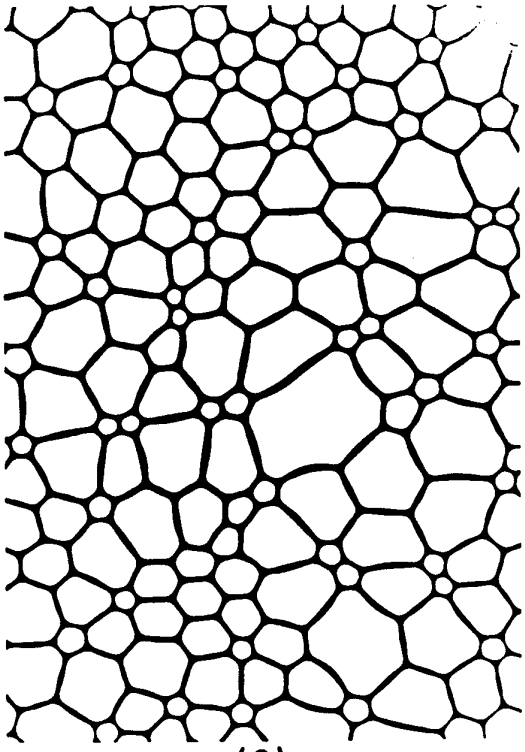

(C)

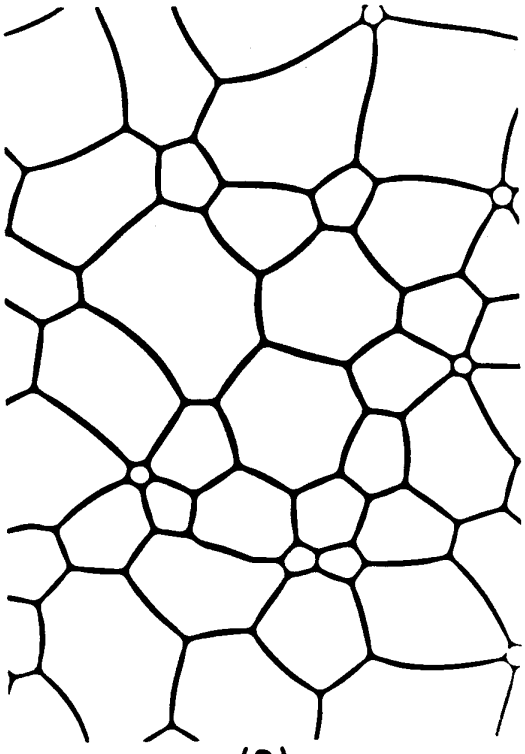

(D)

both the favored ratio between white and black and the selected wavelength, until at some critical field, the last black line collapses and the sample has uniform magnetization. We show an early example of this process by Kooy and Enz in Fig. 56.

In the case of a bubble pattern at a temperature much below T_N, the process is different (See Fig. 57). Because it takes energy to change the topology of a three-connected vertex (to break a wall), bubble patterns cannot change scale smoothly in the way a labyrinth can. If we apply an external field to favor the bubble orientation, the walls initially narrow, but soon reach a size below which they are unstable. The next stage consists of the shrinking of few-sided (small bubbles) but the wall energy prevents small bubbles from shrinking indefinitely. Bubbles that are too small increase in energy when they shrink (hence the absence of three- and four-sided bubbles). These stable uniform area five-sided bubbles freeze the pattern evolution (note the presence of many uniform five-sided bubbles in Fig 57 (A)-(C)). They can also maintain a size much smaller than the optimal wavelength. For the ratio of white to black to increase further the small bubbles must collapse entirely and this is the fundamental mechanism of coarsening in magnetic bubbles. Because of the long range dipole interaction and the pinning of five-sided bubblesi which results in large areas having mismatched wavelength, the reorganization of the pattern tends to happen abruptly, with large patches reorganizing together rather than continuously with bubble by bubble reorganization as in normal coarsening. In particular, five-sided bubbles near

Fig. 58 Coarsening of Magnetic Bubbles. Number of bubbles in a fixed area pattern versus applied magnetic field (Figure supplied by P. Molho 1989).

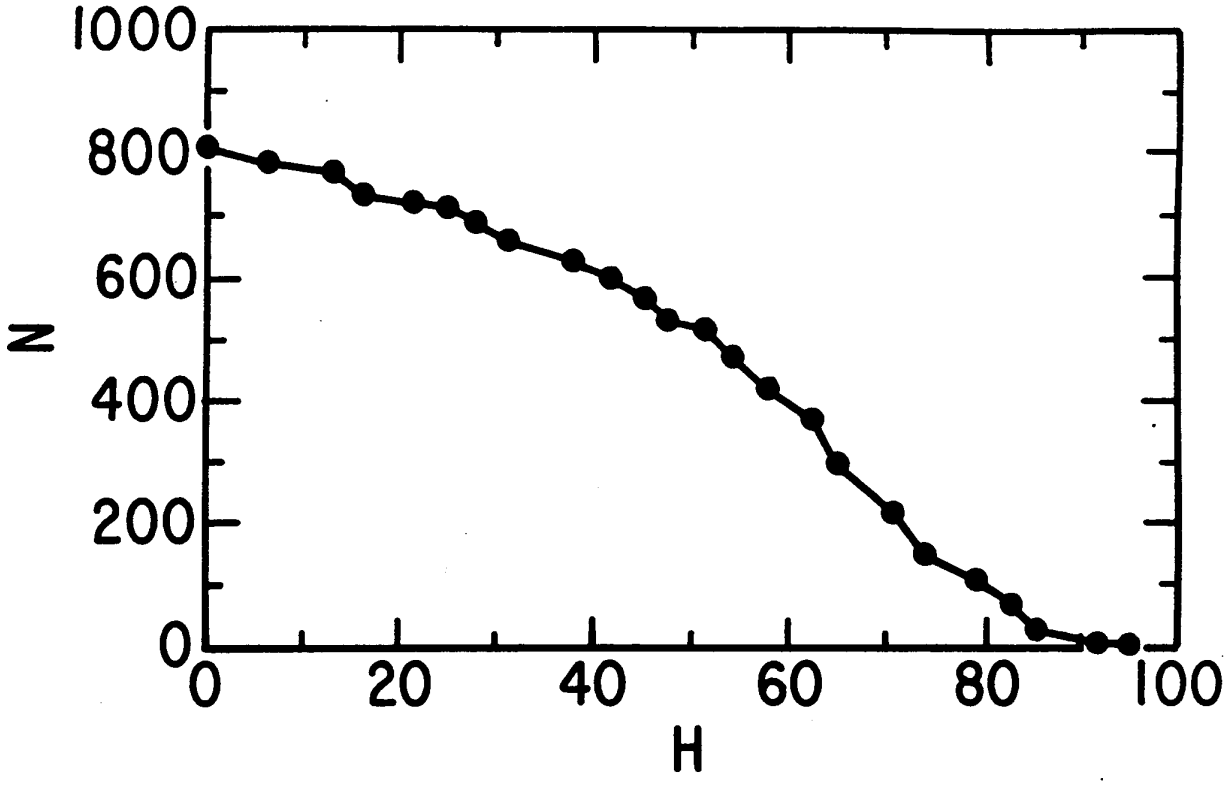
1000
800
600
400
200
0
N
0
20
40
60
80
100
H

Fig. 59 Coarsening of Magnetic Bubbles. Average area per bubble in a bubble pattern versus applied magnetic field (Figure supplied by P. Molho 1989).

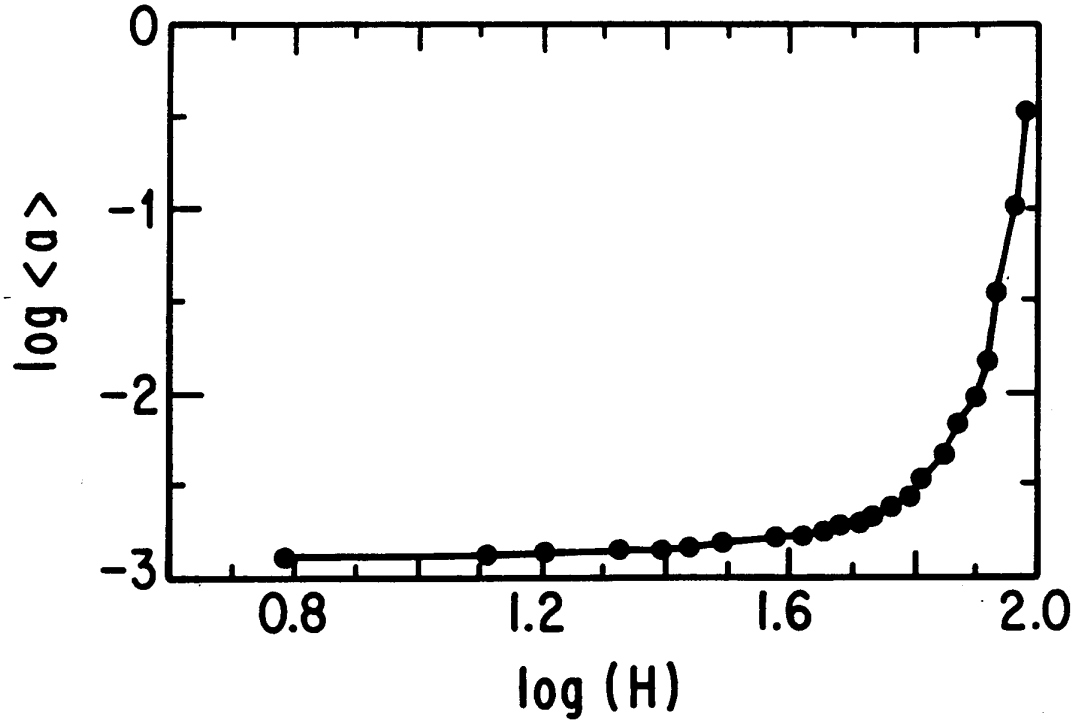
0
-1
-2
-3
log <a>
0.8
1.2
1.6
2.0
log (H)

Fig. 60 Coarsening of Magnetic Bubbles. Moments of the side distribution in a bubble pattern versus applied magnetic field (A) Second moment. (B) Third moment. (C) Fourth moment. (D) Width (Calculated from data supplied by P. Molho 1989)

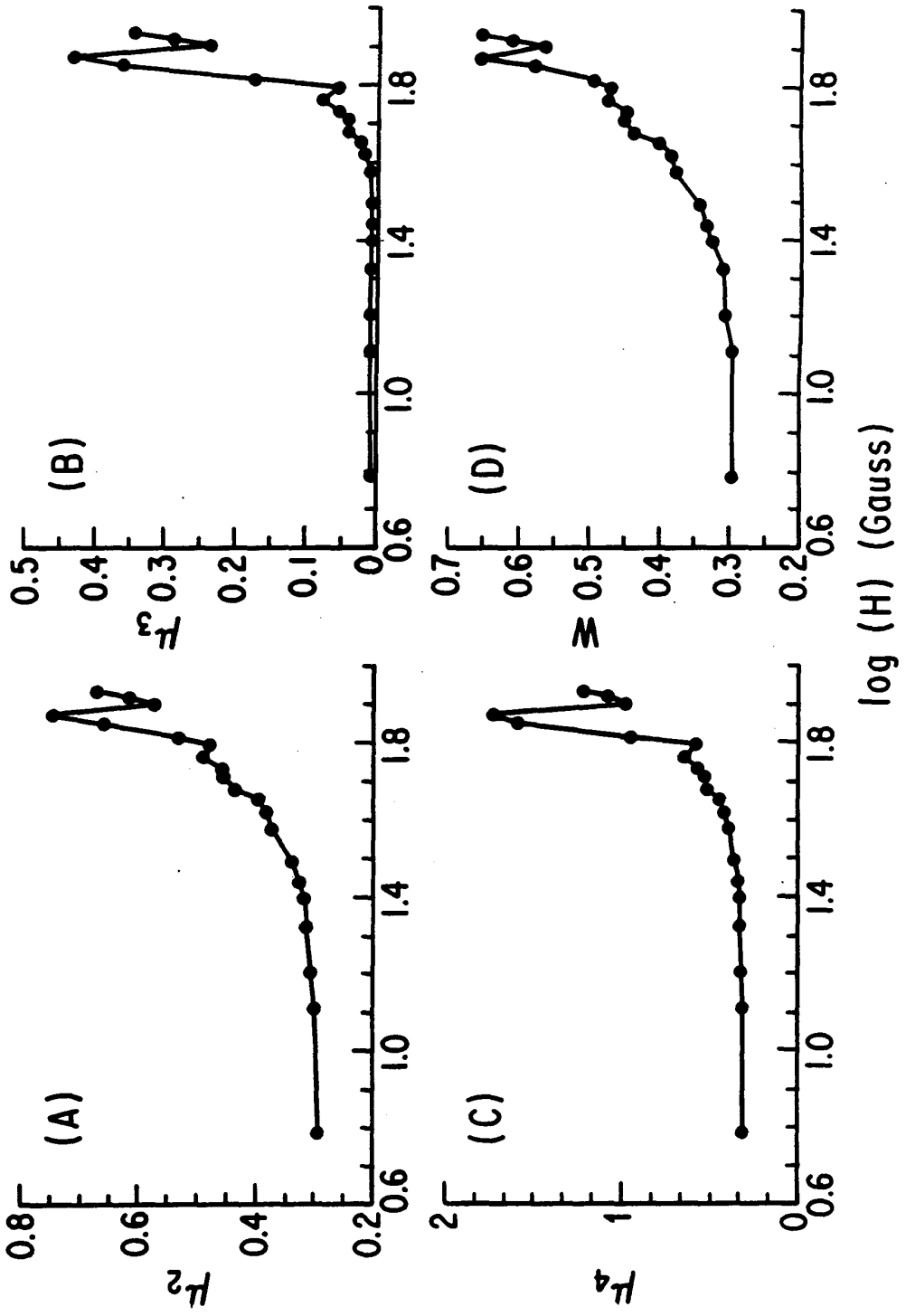
(A)
(B)
(C)
(D)
μ_2
μ_3
μ_4
W
log (H) (Gauss)

Fig. 61 Coarsening of Magnetic Bubbles. Area Distributions. (A) Total area distribution. (B) Area distribution for five-sided bubbles. (C) Area distribution for six-sided bubbles. (D) Area distribution for seven-sided bubbles (Figure supplied by M. Magnasco 1989).

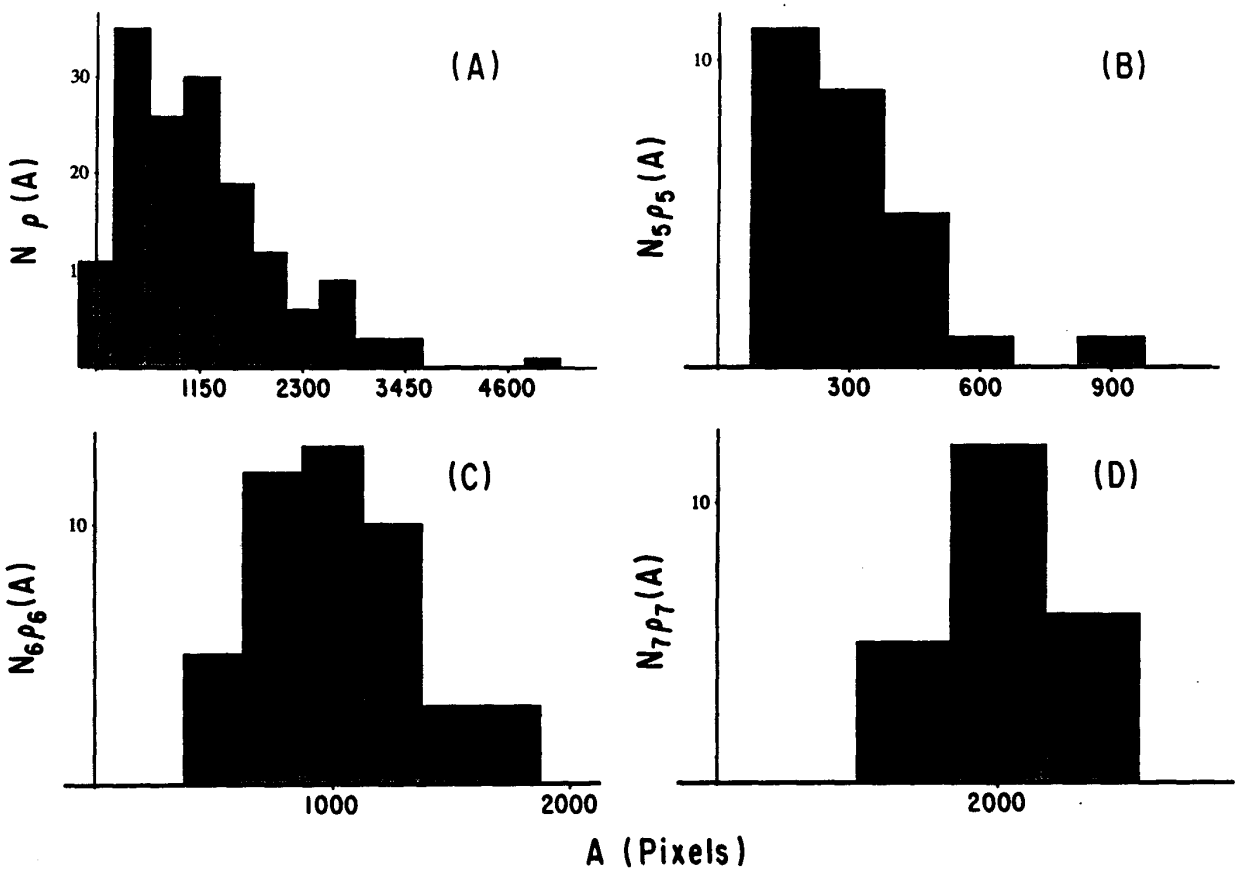
(A)
(B)
(C)
(D)
N ρ (A)
N5ρ5(A)
N6ρ6(A)
N7ρ7(A)
30
20
1
10
10
1150
2300
3450
4600
300
600
900
1000
2000
2000
A (Pixels)

each other tend to be destabilizing so there is a critical field above which groups of three five-sided bubbles lose stablity, then a field above which pairs become unstable, and finally a field above which single five-sided bubbles become unstable. At this field there are no more topological structures to stabilize the pattern and the length scale grows explosively (see Fig. 59). For high applied fields the size of the reorganizing patches is large and wall breakage and domain coalescence are common. One way to make the evolution more like a soap froth is to apply a small alternating bias field on top of the main field.[22]

If we calculate our usual quantities using Molho *et al.*'s measurements for coarsening magnetic bubbles ($< a(H) >$, moments, etc.) we see a very different general pattern from that of the soap froth. The number of bubbles decreased slightly faster than linearly in H (Fig. 58). On a log-log plot, there was a clear but smooth rollover around 50 Gauss, where the rate of area growth suddenly increased (Fig. 59). The monotonic increase of average area with applied magnetic field at least suggests that we are not too far wrong to associate field strength with time. As the field increased, $\rho(6)$ decreased monotonically and $\rho(5)$ and $\rho(7)$ increased monotonically, but the distributions themselves remained very narrow.

The moments all showed the same behavior, with μ_2 gradually increasing from 0.29 to 0.39 before taking off (Fig. 60 (a)), μ_3 staying constant at 0.008 before increasing (Fig. 60 (b)), μ_4 staying nearly constant around 0.33 (Fig. 60 (c)), and W increasing in step with the area from about 0.30 to 0.38

over the same range (Fig. 60 (d)). If we wanted to identify any of these patterns as a scaling state we would have to choose those at low magnetic field, but this seems unsatisfactory. Instead it seems more reasonable to accept that magnetic patterns never find an equilibrium. At all applied magnetic fields six-sided bubbles dominated (except perhaps at very high fields where our statistics are abysmal), there were no three- or four-sided bubbles. Bubbles with more than eight sides were extremely rare and the moments were much smaller than observed in normal coarsening systems, resembling much more the distribution functions we associate with biological materials or basalt fracture. The basic reason is the same in both cases. Wavelength or area selection results in strong limitations on the possible width of the side distributions. The total area distribution (Fig. 61 (A)) resembled that of the soap froth with a few significant differences. As in the soap froth, $\rho(A)$ decreased with increasing area for large areas, but more rapidly as befits a wavelength selected distribution. Unlike the soap froth, the number of very small bubbles was small. Five-sided bubbles (Fig. 61 (B)) formed a well defined class with a well defined non-zero most probable area. Six- and seven-sided bubbles, which do not feel the constraint on minimum bubble size, showed distributions close to those found in the soap froth (Fig. 61 (C) and (D)). To the extent that such a measurement is meaningful for a distribution in which only five- though nine-sided bubbles occur, the patterns appeared to follow the Aboav-Weaire law.

In spite of these differences between magnetic bubbles and our other

coarsening patterns, we can still approximate our coarsening as a competition between surface tension energy minimization and topological constrains. We have already noted the stabilizing effect of five-sided bubbles. In fact, any three-connected vertex is stabilizing in the same way because (at least at temperatures well below the Néel temperature) breaking a wall costs energy.[168] We see this most clearly when we perform the experiment impossible in normal coarsening of increasing and then decreasing the magnetic field. We show Molho *et al.*'s example in Fig. 62. He began with an initial bubble pattern at moderate field and temperature (Fig. 62 (A)) and reduced the magnetic field. Since the pattern could not nucleate new bubbles it adjusted to its smaller optimal wavelength by having its walls buckle and stretch (Fig. 62 (B)). Where the presence of pinned five-sided bubbles resulted in a local wavelength smaller than the optimal, the five-sided bubbles grew but the walls remained smooth (e.g. in the lower middle left of Fig. 62 (B)). Decreasing the applied field to near zero resulted in a labyrinth with almost uniform areas of black and white (Fig. 62 (C)). Looking carefully at Figs. 62 (B) and (C) shows that the three-connected vertices moved slightly but did not disappear. Increasing the field back to its original value restored a pattern topologically close to the original (Fig. 62 (D)). While the sizes of the bubbles changed slightly, most of the vertices remained unchanged. In a few places, bubbles which were much smaller than the optimal wavelength

disappeared. Presumably the changes in pattern detail affected the stability of nearly unstable bubbles as the field was increased, resulting in the disappearance of a few additional bubbles.

For the sake of the pictures and to stimulate further thought on the significance of anisotropy and long range interactions we include a few examples of exotic coarsening behavior for which we do not yet have quantitative analyses.

Near the Néel temperature the presence of a defect in the sample crystal can allow the nucleation of labyrinth at no energy cost. Molho *et al.* began with a pattern at $T = T_N - 5°$ C (Fig. 63 (A)), indistinguishable from that shown in Fig. 56 (a). As they increased the applied field a region of labyrinth nucleated from a defect (Fig. 63 (B)). At higher fields weaker defect centers also began to nucleate labyrinth (Fig. 63 (C)). Finally the labyrinth pushed aside the bubbles to dominate the pattern (Fig. 63 (D)). The wavelength of the labyrinth was substantially larger than the wavelength of the bubbles. It is also interesting to note that this entire evolution took place at fields too small to cause the collapse of bubbles. One could scarcely ask for a clearer demonstration that the labyrinth pattern has a lower energy than the bubble pattern, and that the energy advantage increases with field. The only thing that kept the labyrinth from swallowing the bubbles completely was the boundary of stretched bubbles (looking rather like the epithelium of a tree) which apparently add an extra "domain energy" to the labyrinthine

Fig. 62 Pattern Conservation in Magnetic Bubbles. (A) A bubble pattern at a fixed field, $T = 20°$ C. (B) The field is decreased and the walls buckle. (C) At small fields a nearly symmetric labyrinth forms. (D) Returning the field to its initial value restores the topology of the original pattern with minor changes (Figure supplied by P. Molho 1989).

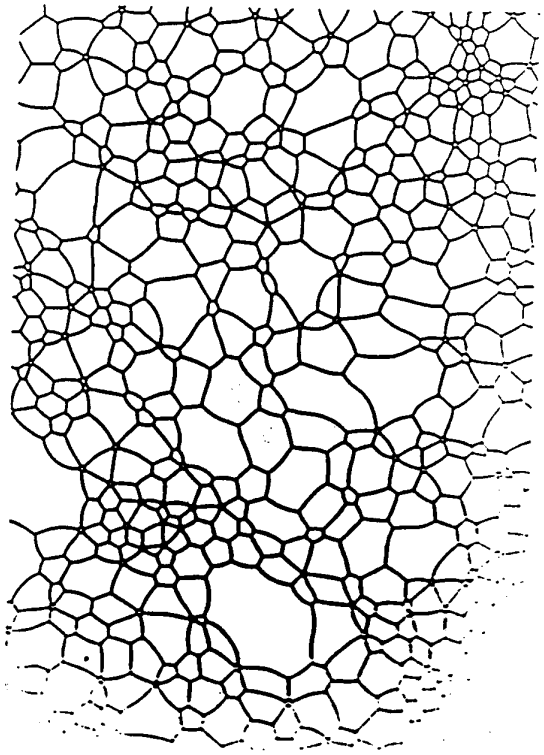

(A)

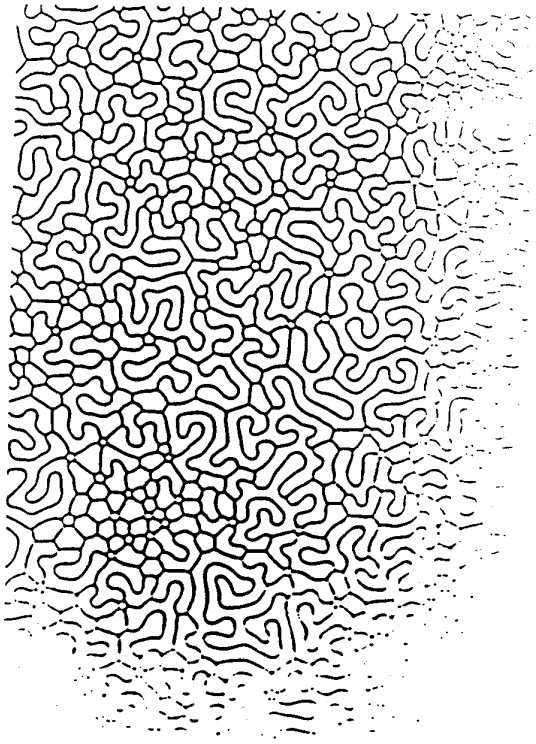

(B)

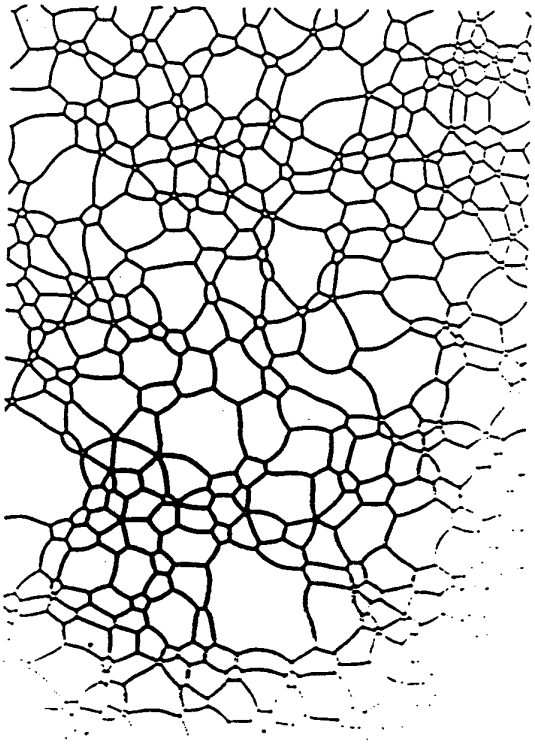

(D)

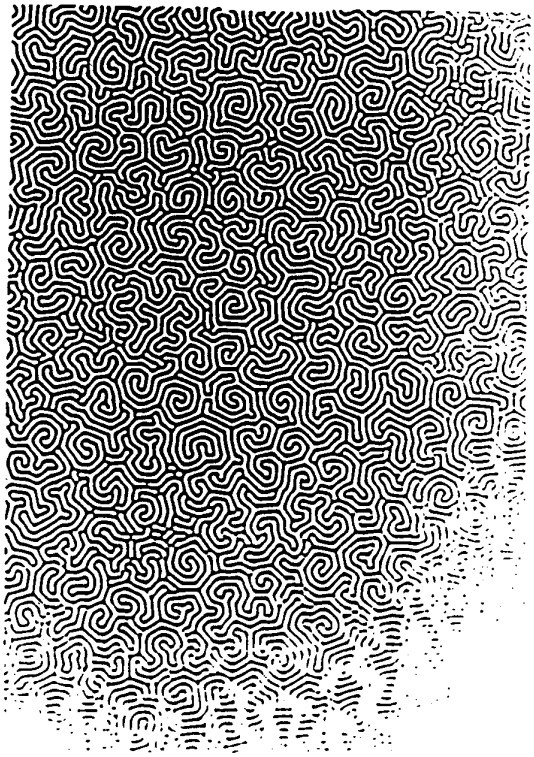

(C)

Fig. 63 Nucleation of Labyrinth. Nucleation of labyrinth from a defect with applied magnetic field, $T = T_N - 5°$ C. (A) H= 0 Oe. (B) H= 17 Oe, beginning of nucleation. (C) H= 19.1 Oe, labyrinth begins to nucleate at additional locations. (D) H= 19.4 Oe, Labyrinth grows rapidly at the expense of bubbles (Figure supplied by P. Molho 1989).

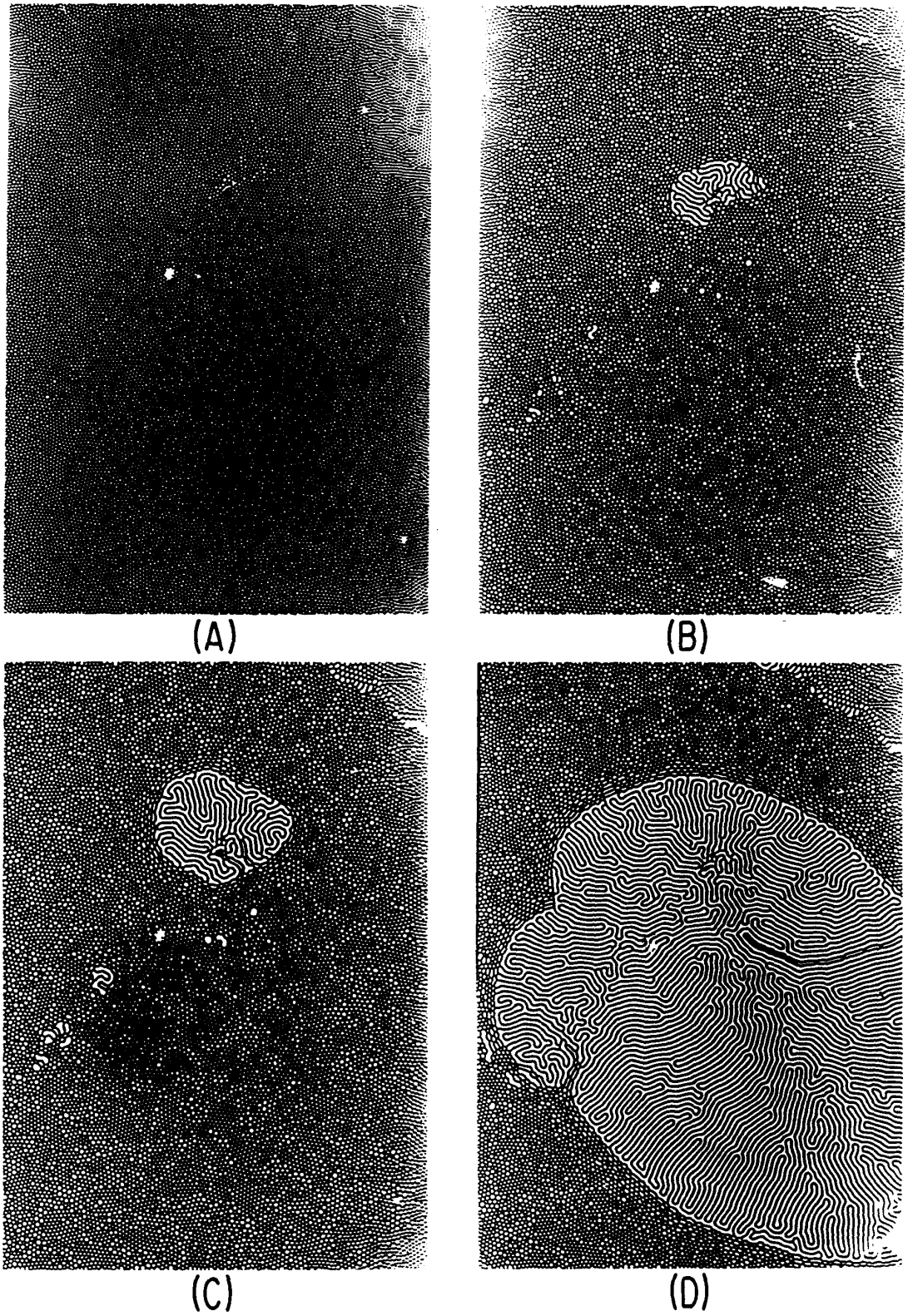
(A)
(B)
(C)
(D)

Fig. 64 Anisotropic Coarsening of Bubbles. Effect of anisotropy on bubble growth near T_N. $T = T_N - 1°$ C. (A) H=16.5 Oe. (B) H=17.5 Oe, bubbles begin to stretch. (C) H=19.0 Oe, growth of elongated bubbles. (D) H=21.5 Oe, bubbles grow by the motion of three-connected vertices to lower left (Figure supplied by P. Molho 1989).

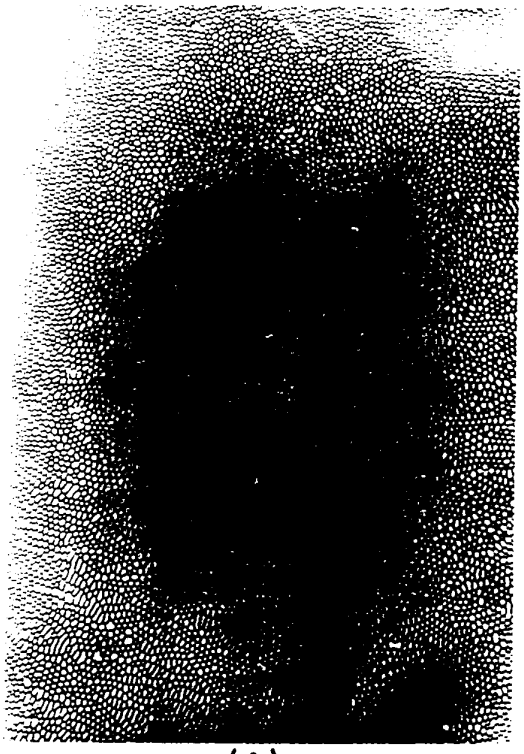

(A)

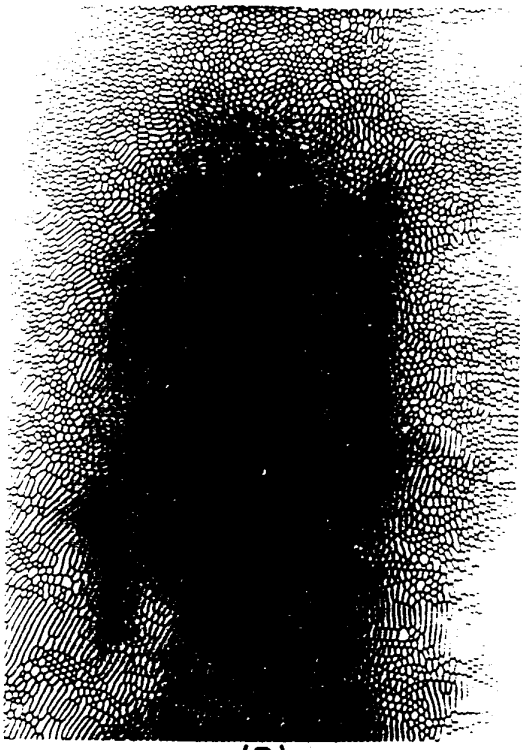

(B)

(C)

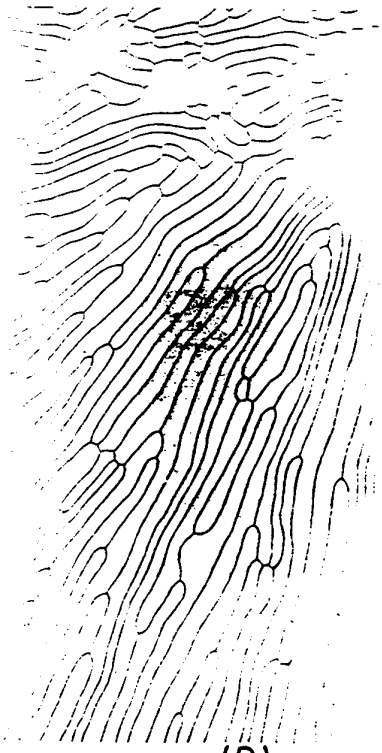

(D)

Fig. 65 Anomalous Bubble Growth in Magnetic Bubbles. Anomalous bubble growth in a magnetic bubble pattern near T_N, $T = T_N - 4°$ C. (A) H= 0 Oe. (B) H= 28 Oe, a few bubbles grow bigger as the field increases. (C) H= 30 Oe. (D) H= 31 Oe, THe larger bubbles grow rapidly. (E) H= 32.1 Oe, the large bubbles dominate the pattern. (F) H= 36 Oe, the initial length scale has disappeared and the pattern resembles that produced by normal bubble growth (Figure supplied by P. Molho 1989).

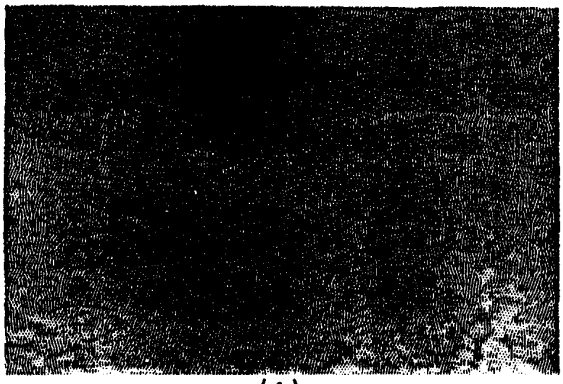

(A)

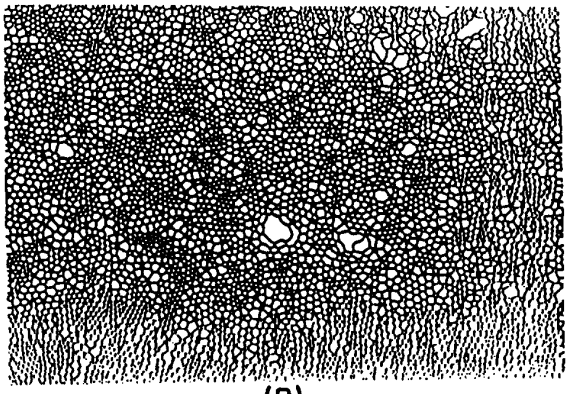

(B)

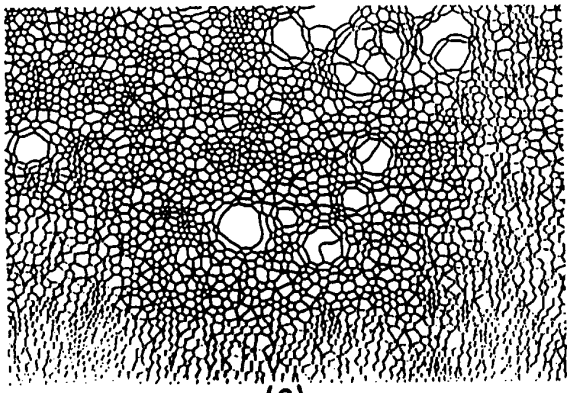

(C)

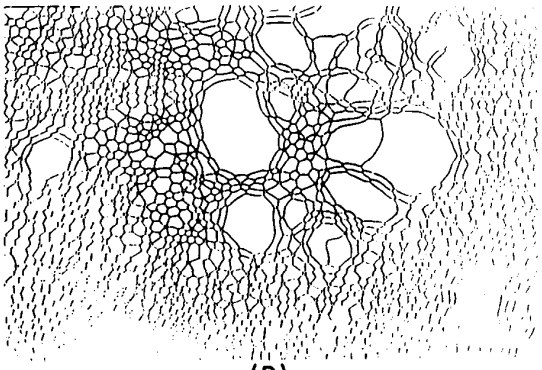

(D)

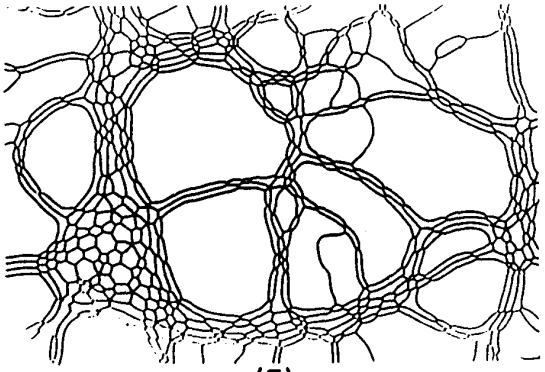

(E)

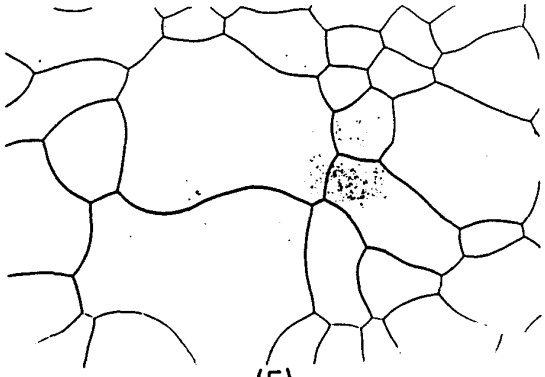

(F)

Fig. 66 Coarsening of Magnetic Bubbles. Bubble growth for the ensemble of n-sided bubbles as a function of applied magnetic field. Note that this is not the same as von Neumann's law (Figure supplied by M. Magnasco 1989).

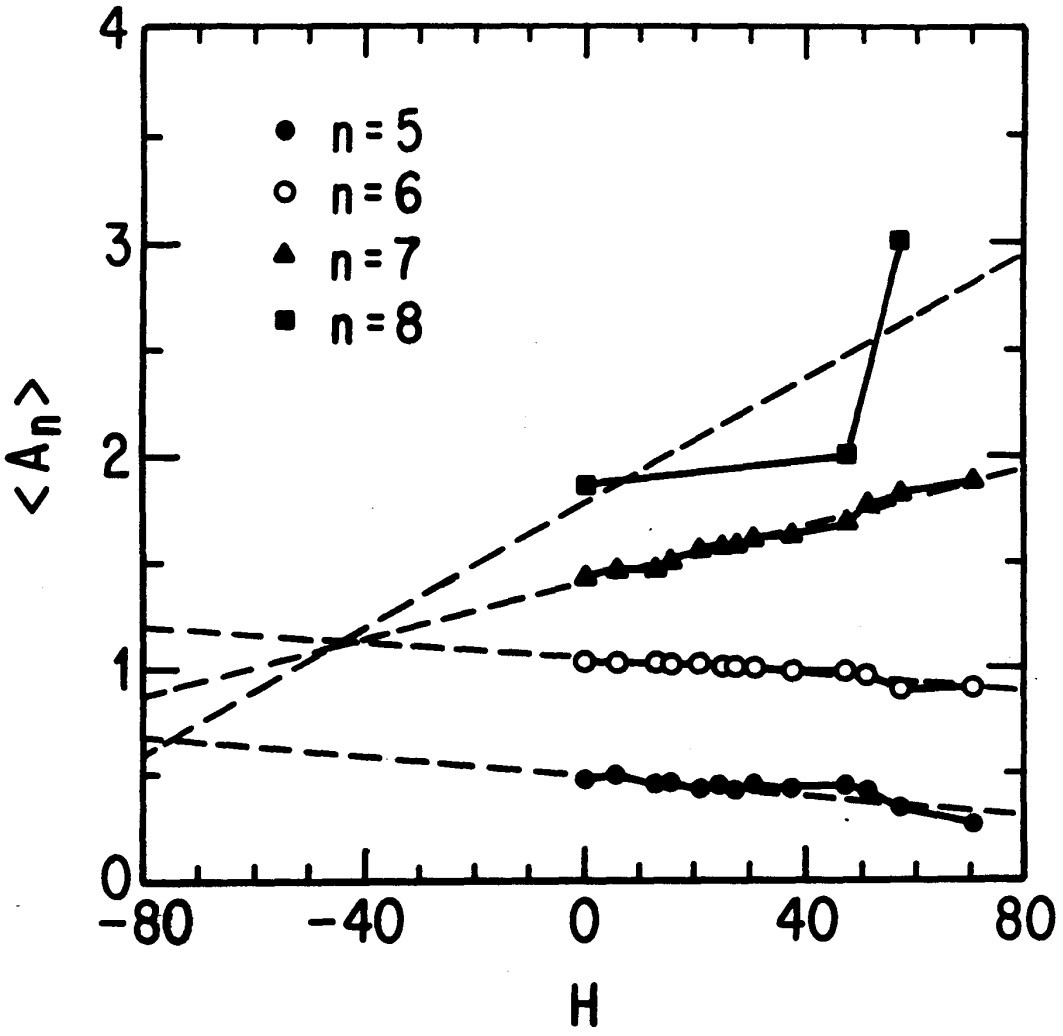
4
3
2
1
0
-80
-40
0
40
80
H
<A_n>
n=5
n=6
n=7
n=8

patch. However, besides retarding the growth of the labyrinth, these bubbles also facilitate the collapse of the original bubble pattern. In their absence the nucleated pattern cannot grow.[167] The temperature determines whether the labyrinth is energetically favorable enough to cause wall breakage.

Anisotropy can also have a decisive effect on coarsening. In Fig. 64 we show Molho *et al.*'s observation of coarsening in a material at $T = T_N - 1°$ C, which allowed walls with a particular orientation to break more easily (ranging from east-west at the right of the picture to northwest -southeast at the upper left). Because this type of anisotropy is small the effect occurs only near T_N where the wall breakage energy is very small. Once again the zero field pattern (Fig. 64 (A) was indistinguishable from Fig. 56 (a). As the field was increased however, bubbles with borders aligned along easy breaking directions began to coalesce (Fig. 64 (B)), producing a pattern of elongated bubbles reminiscent of cloth stretched near the point of failure. For larger fields the coalescence perpendicular to the preferred direction continued (Fig. 64 (C)), eventually producing a strongly grained pattern which grew by the sliding of three-fold vertices (Fig. 64 (D)). The final pattern was nearly as well behaved as one composed of well ordered parallel stripes.

Finally we show Molho *et al.*'s example of orientationally isotropic but spatially varying rates of bubble growth, analogous to the case of anomalous grain growth in metals. Again, working near T_N is crucial since the small anisotropy can only have an effect when it is comparable to the wall breakage energy. A sample that exhibits anomalous bubble growth near T_N will show

normal bubble growth at lower temperatures. They began with the usual zero field bubbles at $T = T_N - 4°$ C (Fig. 61 (A)). For small fields they observed normal grain growth with a few bubbles slightly larger than their neighbors (Fig. 61 (B)). As the field increased further these larger bubbles grew explosively at the expense of their neighbors (Fig. 61 (C)-(E)) producing the characteristic bark-like pattern of elongated bubbles lying along the surface of the growing bubbles which we noted in Fig. 11 (D). Finally the anomalously growing bubbles swallowed all the small length scale pattern and returned to a situation indistinguishable from that produced by normal bubble growth (Fig. 61 (F) compare Fig. 56 (d)). This return to a normal looking scaling pattern is also observed in metals. Of course if we were to look at the distribution functions for this pattern as a function of field they would be bimodal, and vastly broader than the corresponding stages in normal growth. The energy to drive this anomalous grain growth presumably comes from the mismatch between the wavelength of the bubble pattern and the optimal wavelength, but the mechanism which selects the anomalously growing grains is unclear.

Existing theories of magnetic bubbles treat either regular arrays or isolated bubbles. There have also been a few attempts to deduce large scale statistical properties of random lattices. The difficulties are several. Since bubbles evolve in patches and wall breakage is a dominant mechanism in some types of coarsening, we do not expect a simple description like our network models to suffice. In extreme cases the growth or shrinkage of an

individual bubble becomes an ill defined concept. Surprisingly if we take the naive zeroth order approximation to measuring von Neuann's law we obtain a sensible result. In Fig. 66 we plot Molho *et al.*'s measurement for the average total area of n-sided bubbles as a function of applied external field. This measurement is not equivalent to von Neumann's law because bubbles can change their number of sides. If we note that $< A_n >= \lambda_n < a >$ we obtain simply:

$$\frac{d < A_n >}{d\mathrm{H}} = \lambda_n \frac{d < a >}{d\mathrm{H}} + < a > \frac{d\lambda_n}{d\mathrm{H}}. \qquad \text{(X.4)}$$

In a scaling state soap froth it would show that all bubbles grow with a rate $\frac{d<A_n>}{dt} = \kappa\lambda_n$. For the magnetic bubbles the result is rather different. Average bubble areas, $< A_n >$, do depend linearly on applied magnetic field (which we might not have predicted looking at the nonlinear dependence of total area), but five- and six-sided bubbles shrink and seven- and eight-sided bubbles grow, showing that the distributions continue to evolve. This gives us a relation between $< a >$ and λ_n:

$$\frac{d \ln < a >}{d\mathrm{H}} + \frac{d \ln \lambda_n}{d\mathrm{H}} = \frac{\kappa}{\lambda_n < a >}, \qquad \text{(X.5)}$$

but tells us nothing about the evolution of individual bubbles. Whether this relation will prove useful in developing a theory for magnetic bubble growth remains to be seen. It may prove more helpful as a way to test theories than to create them.

Magnasco has written an interaction model mean field theory for the rapid equilibration of a bubble pattern after a field change and during nucleation at the Néel temperature, taking into account both separations and

radii of the form and assuming nearly circular bubbles.[154] He defined the mean field distance between the surfaces of two bubbles to be

$$d_{ij} \equiv |\vec{x}_i - \vec{x}_j| - r_i - r_j, \tag{X.6}$$

where $\vec{x}_i$ is the position of the center of the ith bubble and r_i its radius. Then he took the movement of the centers of the bubbles to be the effect of the dipole repulsion by the remaining bubbles,

$$\frac{d\vec{x}_i}{t} = \kappa_1 \sum_{j \neq i} \frac{\vec{x}_i - \vec{x}_j}{d_{ij}^3}, \tag{X.7}$$

and the change in radius to be pressure driven by the same dipole force,

$$\frac{dr_i}{dt} = \kappa_2 \sum_{j \neq i} (1 - \frac{1}{d_{ij}^3}), \tag{X.8}$$

where κ_2 controls the equilibrium width of the area distribution, small κ_2 resulting in broad distributions and large κ_2 in narrow distributions. Note the nonlinearity in both terms of the equation. He obtained good agreement with experiment for the qualitative equilibration but has not yet measured the distribution functions. In principle κ_2 should be a decreasing function of the applied magnetic field, and Magnasco is currently developing a model for the field evolution of magnetic bubble patterns using an extended model of this type. The difficulty is in understanding why a model that should work well for Bragg's bubble rafts should also be appropriate in a case where wall breakage and patch rearrangement are important mechanisms.

We could also write a boundary dynamic model along the lines of Frost and Thompson, adding either an exact integrated form for the local magnetization or the mean field version given in equation X.7. It should be possible

to include wall breakage and the stabilization of five-sided bubbles with an auxiliary field. The collapse of finite size bubbles can also be included by increasing the length scale for bubble removal to a larger value. While the Potts model seems like the natural type of model for a magnetic system, the calculation of the local magnetization seems guaranteed to be computationally prohibitive. Perhaps, it would be possible to used a mixed model like that of Weaire and Kermode with Potts model calculations layered on top of a mean field calculation of the local magnetization.